IOPscience iopscience.iop.org

Home Search Collections Journals About Contact us My IOPscience

Ground-state structure and thermodynamics of Yukawa Bose fluids in dimensionality $D = 3$ and $D = 2$

This article has been downloaded from IOPscience. Please scroll down to see the full text article.

1998 J. Phys.: Condens. Matter 10 11645

(http://iopscience.iop.org/0953-8984/10/50/005)

View the table of contents for this issue, or go to the journal homepage for more

Download details:
IP Address: 171.66.16.210
The article was downloaded on 14/05/2010 at 18:13

Please note that terms and conditions apply.

J. Phys.: Condens. Matter **10** (1998) 11645–11658. Printed in the UK PII: S0953-8984(98)96339-1

Ground-state structure and thermodynamics of Yukawa Bose fluids in dimensionality $D = 3$ and $D = 2$

E Strepparola, R Nifosì and M P Tosi

Istituto Nazionale di Fisica della Materia and Classe di Scienze, Scuola Normale Superiore, Piazza dei Cavalieri 7, I-56126 Pisa, Italy

Received 14 September 1998

Abstract. We evaluate the structure and the thermodynamic properties (internal energy, pressure and compressibility) of zero-temperature fluids of Bose particles interacting via the Yukawa potential in dimensionality $D = 3$ and $D = 2$. These systems provide simplified models for nuclear matter in $D = 3$ and for assemblies of flux lines in high-T_c superconductors in $D = 2$. Our calculations are based on the dielectric formalism, with short-range correlations being treated in the self-consistent scheme of Singwi *et al*. In both dimensionalities our results for the ground-state energy demonstrate a crucial role of short-range correlations and are in good agreement with those of variational and diffusion Monte Carlo studies over extended ranges of values for the system parameters (reduced DeBoer length and reduced particle density). Reasonable agreement is also found for the pressure with the available diffusion Monte Carlo data in $D = 2$. The extent of the deviations from the compressibility sum rule in the theory is assessed for both dimensionalities. On all the above grounds it appears that the present approach is quite accurate for the high-density fluid and provides a useful starting point for fully quantitative studies of the low-density fluid.

1. Introduction

The Yukawa potential presents a combination of short range with soft core, in contrast with stiff-core repulsions (short-range and hard) and with bare Coulomb repulsions (long-range and soft). In dimensionality $D = 3$ it takes the form $V_3(r) = (\varepsilon\sigma/r)\exp(-r/\sigma)$, where ε is an energy scale and σ is a length scale having the meaning of a screening length, while in $D = 2$ it is given by $V_2(r) = \varepsilon K_0(r/\sigma)$ with $K_0(x)$ the modified Bessel function, which decays as $x^{-1/2}\exp(-x)$ at large distance and behaves as $-\ln(x)$ at short distance. The latter behaviour describes the bare Coulomb interaction in a two-dimensional world. The corresponding forms of the Fourier transforms are $V_3(q) = 4\pi\varepsilon\sigma^3/(1 + q^2\sigma^2)$ and $V_2(q) = 2\pi\varepsilon\sigma^2/(1 + q^2\sigma^2)$.

Numerical evaluations of the ground state of fluids of Bose particles interacting via the Yukawa potential (for short, Yukawa Bose fluids or YBF) have been reported by Ceperley and coworkers [1–3] from the application of quantal Monte Carlo (QMC) simulations. The phase diagrams that they found show a solid phase which is stable at sufficiently strong couplings and melts on expansion or compression. The motivation for studies of the 3D-YBF comes from models for the interior of pulsars and dense nuclear matter, the background to this field being given in exhaustive detail in a review article of Baym and Pethick [4]. Interest in the 2D-YBF is more recent and has been greatly stimulated by the work of Nelson and Seung [5, 6], who showed that a fluid of flux lines in strongly type-II

0953-8984/98/5011645+14$19.50 © 1998 IOP Publishing Ltd

superconducting materials can be mapped onto this system. Following an early variational Monte Carlo study [7], the transition from an Abrikosov lattice to a liquid of vortices has been studied by the dislocation mechanism of melting [8] and by the density functional theory of freezing [9, 10]. A first-order transition to a bosonic superfluid of entangled flux lines has been reported in a very recent study by the path-integral Monte Carlo method [11].

In the present work we aim at developing the many-body theory of the ground-state properties of the YBF in both $D = 3$ and $D = 2$. Our main focus is on evaluating the ground-state thermodynamic properties of these fluids over wide ranges of system parameters near the phase boundary and on testing the quality of the results against the Monte Carlo simulation data of Ceperley *et al* [2, 3]. The calculations are carried out within the dielectric formalism by means of the so-called STLS scheme of Singwi *et al* [12], which embodies self-consistency in the evaluation of the ground-state pair distribution function $g(r)$ from the dynamic structure factor of the fluid via the fluctuation–dissipation theorem. In turn, in the case of pair potentials the internal energy and the equation of state at zero temperature can be obtained from $g(r)$ via integration over the coupling strength. The usefulness of this approach for this type of calculation has been proven by previous work on a variety of quantal fluids, including fluids of charged bosons in $D = 3$ [13, 14] and in $D = 2$ [13, 15, 16]. In addition, the STLS approach has been very recently used to study the ground-state structure of the 2D-YBF [17].

The layout of the paper is briefly as follows. Section 2 introduces the essential equations of the dielectric formalism and sets out their evaluation in the STLS approximation. Various results for the structure and the elementary excitations of the 3D-YBF are reported in section 3, similar results for the 2D-YBF having already been given in [17]. Our numerical results for the ground-state energy and for the equation of state in both dimensionalities are reported and discussed in sections 4 and 5, respectively. We conclude with a brief summary in section 6.

2. Linear density response

The Hamiltonian of the system can be written as

$$H = -\sum_i \Lambda^{*2}\nabla_i^2 + \sum_{i>j} v_D(r_{ij}) \tag{1}$$

after taking σ as the unit for lengths and ε as the unit for energies. Here, $v_3(x) = x^{-1}\exp(-x)$, $v_2(x) = K_0(x)$ and Λ^* is the DeBoer parameter, which is defined as

$$\Lambda^* = (\hbar^2/2m\varepsilon\sigma^2)^{1/2}. \tag{2}$$

Λ^* is a measure of the kinetic energy relative to the strength of the interactions (notice that for the 3D-YBF our definition of Λ^* is smaller than that of Ceperley *et al* [2] by a factor $2\pi\sqrt{2}$).

In addition to Λ^*, the only other system parameter at $T = 0$ is the particle density n as described by the reduced density $\rho = n\sigma^D$.

2.1. Dielectric formalism in the static-local-field approximation

The linear density response function $\chi(q, \omega)$ of the Bose fluid is written in the form

$$\chi(q, \omega) = \frac{\chi_0(q, \omega)}{1 - V_D(q)[1 - G(q)]\chi_0(q, \omega)} \tag{3}$$

where $\chi_0(q,\omega)$ is the density response function of the ideal Bose gas and $G(q)$ is the local field factor which accounts for short-range correlations in a static approximation [18]. Here,

$$\chi_0(q,\omega) = \frac{2n\varepsilon(q)}{\omega(\omega+\mathrm{i}\eta)-\varepsilon^2(q)} \tag{4}$$

with $\varepsilon(q) = q^2/2m(\hbar = 1)$ and $\eta = 0^+$. Equation (4) assumes that at $T = 0$ all particles in the ideal Bose gas are in the ground state at zero energy.

The excitation spectrum which is obtained from equations (3) and (4) consists of a single collective mode at an energy $E(q)$ given by

$$E(q) = \left\{ \frac{\pi n\varepsilon(2\sigma)^D[1-G(q)]}{1+q^2\sigma^2}\varepsilon(q) + \varepsilon^2(q) \right\}^{1/2}. \tag{5}$$

The dispersion relation in equation (5) reduces in the long-wavelength limit to that of acoustic phonons, $E(q) \to cq$. The value c of the speed of sound is related to the compressibility K by $c = (mnK)^{-1/2}$, where

$$K^{-1} = \tfrac{1}{2}\pi(2\sigma)^D n^2\varepsilon[1-G_0] \tag{6}$$

with $G_0 \equiv G(q=0)$. The same value for the compressibility is obtained from the static density response function in the long-wavelength limit through the relation

$$\lim_{q\to 0} \chi(q,\omega=0) = -n^2K. \tag{7}$$

Therefore, consistency between static and dynamic compressibility is ensured by the theory, irrespectively of the specific choice of the local field factor. Consistency with the thermodynamic compressibility in the STLS approach will be tested in section 5 below.

In connection with the above result we stress that, unlike the case of charged fluids, the quantity G_0 in equation (6) does not vanish for the YBF. This fact implies that short-range correlations play a role already in the long-wavelength properties of the YBF, as is easily understood if one thinks of the Yukawa potential as a screened Coulomb potential in a plasma. We find in our calculations that the value of G_0 decreases towards zero as the reduced density ρ is increased: namely, the Coulombic regime is regained as the interparticle distance becomes much shorter than the screening length. Only in that regime does the random phase approximation (RPA), which sets $G(q) = 0$, become correct at long wavelengths.

The other important quantity that is easily calculated from equations (3) and (4) is the structure factor $S(q)$, through the fluctuation–dissipation theorem

$$S(q) = -(n\pi)^{-1}\int_0^\infty \mathrm{d}\omega\, \mathrm{Im}\,\chi(q,\omega). \tag{8}$$

The result is

$$S(q) = \{1 + 4nmV_D(q)q^{-2}[1-G(q)]\}^{-1/2}. \tag{9}$$

In particular, the long-wavelength behaviour of the structure factor follows in the form

$$\lim_{q\to 0} S(q) = q\Lambda^*[2^D\pi\rho(1-G_0)]^{-1/2}. \tag{10}$$

Equation (9) provides a relationship between the local field factor and the structure factor, which will be used below to enforce self-consistency according to the STLS scheme.

2.2. STLS equations

The STLS approach makes use of a second relationship between the local field factor and the structure factor, which was originally established [12] through an approximate decoupling in the hierarchy of equations of motion for the Wigner distribution functions. For the YBF this relationship reads

$$G(q) = \frac{1}{(2\pi)^D n} \int \mathrm{d}^D q' \frac{\boldsymbol{q}\cdot\boldsymbol{q}'}{q^2} \frac{V_D(q')}{V_D(q)} [1 - S(|\boldsymbol{q} - \boldsymbol{q}'|)]. \tag{11}$$

Equations (9) and (11) are to be solved in a self-consistent manner. After performing the angular integrals in equation (11) and with wavenumbers scaled by the length σ, we find

$$S(q) = \left\{ 1 + \frac{2^D \pi \rho}{\Lambda^{*2} q^2 (1+q^2)} [1 - G(q)] \right\}^{-1/2} \tag{12}$$

and

$$G(q) = \frac{1+q^2}{\rho q^2} \int_0^\infty k^{D-1}\, \mathrm{d}k \Pi_D(q,k)[1 - S(k)] \tag{13}$$

where

$$\Pi_3(q,k) = (2\pi)^{-2} \left[1 + \frac{1+k^2-q^2}{4qk} \ln \frac{1+(q-k)^2}{1+(q+k)^2} \right] \tag{14}$$

and

$$\Pi_2(q,k) = (4\pi)^{-1} \left[1 - \frac{1+k^2-q^2}{\sqrt{(1+q^2+k^2)^2 - 4k^2q^2}} \right]. \tag{15}$$

The numerical solution of equations (12) and (13) will be reported in section 3 below.

The value of G_0 follows from the $q \to 0$ limit of equation (13) as

$$G_0^{(D=3)} = \frac{1}{6\pi^2 \rho} \int_0^\infty \mathrm{d}k \frac{3k^2 + k^4}{(1+k^2)^2} [1 - S(k)] \tag{16}$$

in $D = 3$ and

$$G_0^{(D=2)} = \frac{1}{4\pi\rho} \int_0^\infty \mathrm{d}k \frac{2k}{(1+k^2)^2} [1 - S(k)] \tag{17}$$

in $D = 2$.

On the other hand, the asymptotic values of the local field factor are obtained from equation (13) using the q^{-1} expansion of $\Pi_D(q,k)$ and are simply related to the value of the pair distribution function $g(r)$ at $r = 0$:

$$G(\infty) = 1 - g(0). \tag{18}$$

As usual, the pair distribution function is related to the structure factor by

$$g(r) = 1 + \rho^{-1}(2\pi)^{-D} \int \mathrm{d}^D q [S(q) - 1] \exp(\mathrm{i}\boldsymbol{q}\cdot\boldsymbol{r}). \tag{19}$$

Finally, the large-q behaviour of the structure factor is determined by the value of $G(\infty)$ as

$$S(q \to \infty) = 1 - \frac{2^D \pi \rho [1 - G(\infty)]}{\Lambda^{*2}} q^{-4} \tag{20}$$

according to equation (12).

3. Local field factor, structure and elementary excitations of the 3D-YBF

We report in this section the results of the numerical solution of the STLS equations for the 3D-YBF. For similar results on the 2D-YBF the reader is referred to the work of Bulutay *et al* [17].

Figures 1 and 2 report the local field factor $G(q)$ at two values of the DeBoer parameter and at various values of the reduced density. The pairs of values for (Λ^*, ρ) chosen in these figures are the same as in QMC runs [2] near the phase boundaries between the fluid and the solid. The evolution of G_0 towards the bare Coulomb regime with increasing ρ and the closeness of $G(\infty)$ to unity, implying $g(r) \approx 0$ as $r \to 0$, are evident from these figures.

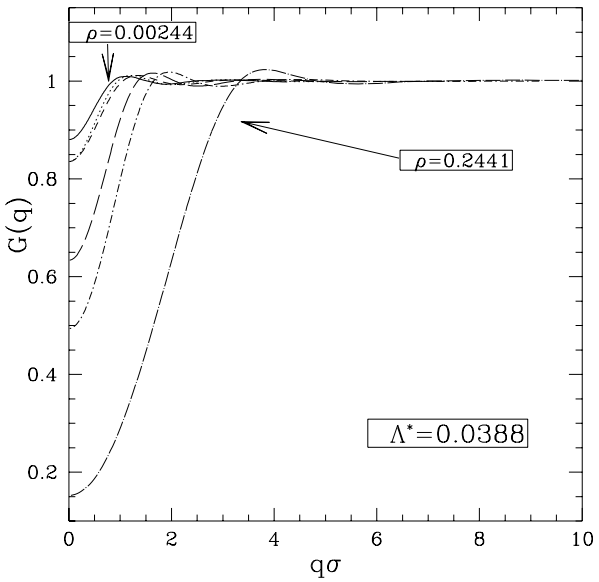

Figure 1. Local field factor $G(q)$ versus $q\sigma$ for the 3D-YBF at $\Lambda^* = 0.0388$ and various values of ρ. Curves at $\rho = 0.002\,44$, $0.003\,66$, $0.004\,88$, 0.0122, 0.0244 and 0.2441 are plotted sequentially, with the smallest and largest value of ρ being indicated.

Figures 3 and 4 report the structure factor $S(q)$ at the same values of system parameters. With increasing ρ the position of the main peak in $S(q)$ moves to larger values of q and its height shows a re-entrant behaviour. The latter feature reflects the nature of the solid–fluid phase diagram established in the QMC work [2]: below a threshold value of Λ^* for crystallization a low-density fluid and a high-density fluid enclose the solid phase, so that the short-range order must decrease as one moves in the fluid phase at constant Λ^* towards both higher and lower densities. The same features are indeed evident also from our results for the pair distribution function $g(r)$, which are reported in figures 5–7.

Figures 8 and 9 show a comparison of our results for $S(q)$ and $g(r)$ with the QMC data of Ceperley *et al* [2]. The structural role of short-range correlations in the 3D-YBF is emphasized through the inclusion of the RPA results: in this case any structure is lacking in $S(q)$, while $g(r)$ shows a deep negative region at short interparticle separations. It appears from these figures that in the STLS approach these correlations are still underestimated at a quantitative level.

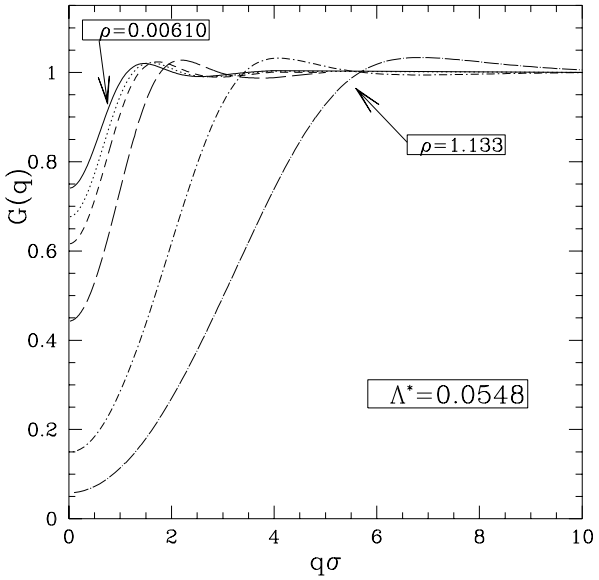

Figure 2. The same as in figure 1, for $\Lambda^* = 0.0548$ and $\rho = 0.00610$, 0.00884, 0.01221, 0.0298, 0.2441 and 1.133.

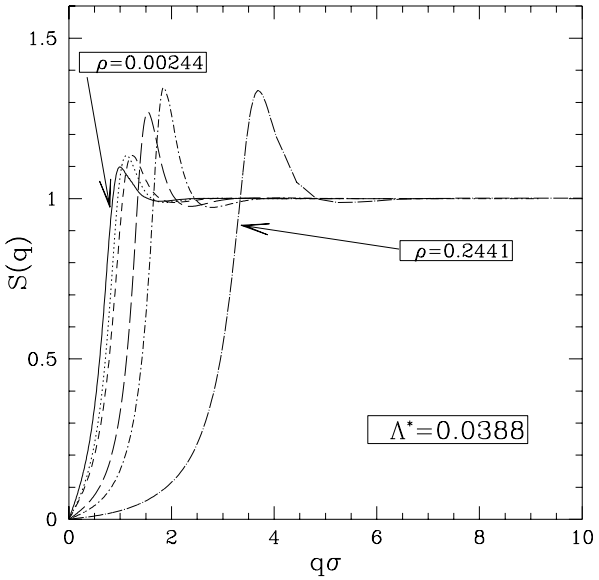

Figure 3. Structure factor $S(q)$ versus $q\sigma$ for the 3D-YBF at the values of the system parameters used in figure 1.

Finally, figure 10 shows an example of the dispersion curve of the collective modes of the 3D-YBF for various reduced densities in the small-Λ^* (strong-coupling) regime. From equation (5) the long-wavelength behaviour of the dispersion curve can be written as

$$E(q) = cq(1 - \alpha q^2) + 0(q^5) \tag{21}$$

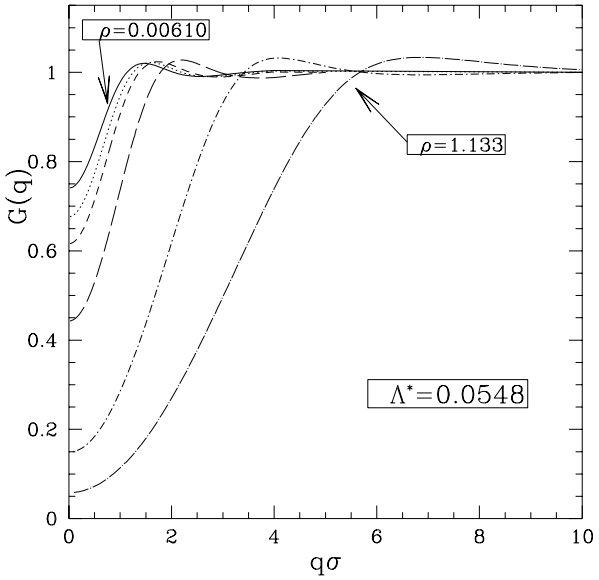

Figure 4. Structure factor $S(q)$ versus $q\sigma$ for the 3D-YBF at the values of the system parameters used in figure 2.

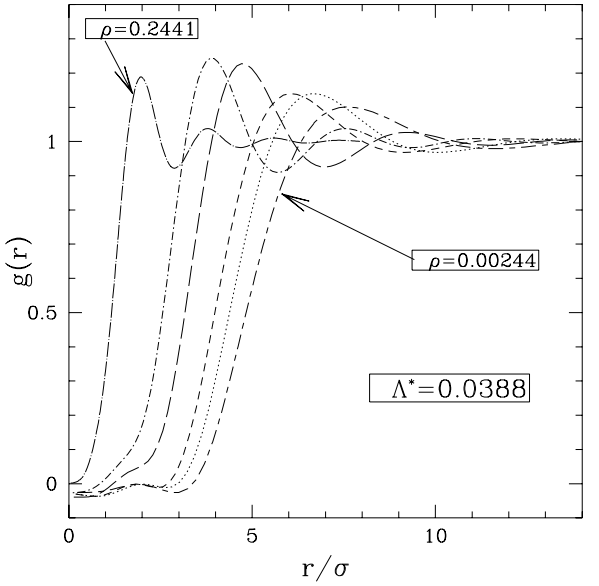

Figure 5. Pair distribution function $g(r)$ versus r/σ for the 3D-YBF at the values of the system parameters used in figure 1. Notice the inversion in the sequence of values of ρ relative to figures 1–4.

where $c = \Lambda^*[2^D\rho\pi(1-G_0)]^{1/2}$ (see equation (6)) and the quantity α is given by

$$\alpha = \frac{1}{2}\left[1 + \frac{G_2}{1-G_0} - \frac{\Lambda^{*2}}{2^D\pi\rho(1-G_0)}\right] \tag{22}$$

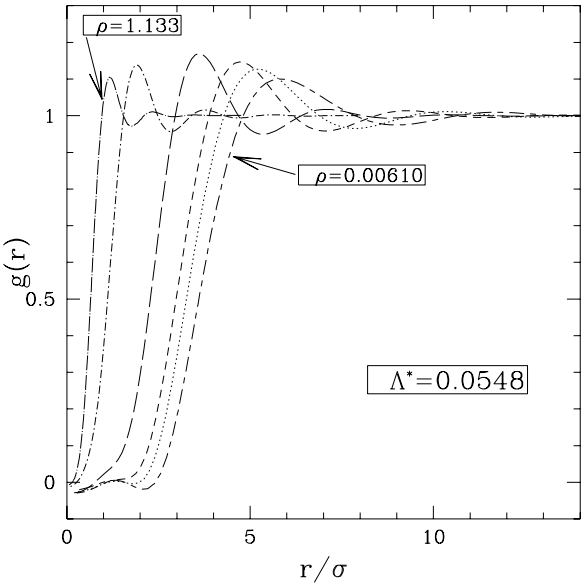

Figure 6. Pair distribution function $g(r)$ versus r/σ for the 3D-YBF at the values of the system parameters used in figure 2.

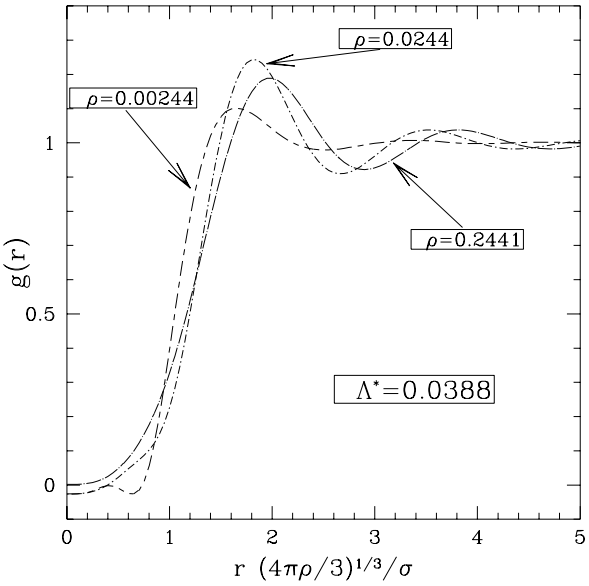

Figure 7. Pair distribution function $g(r)$ of the 3D-YBF versus r in units of the mean interparticle distance, at $\Lambda^* = 0.0388$ and $\rho = 0.002\,44$, 0.0244 and 0.2441.

with G_2 the coefficient of the q^2 term in a Taylor expansion of $G(q)$. It is evident from figure 10 that the free-particle parabola is coming to play a dominant role in the dispersion curve as the density of the fluid decreases towards the dilute-gas regime.

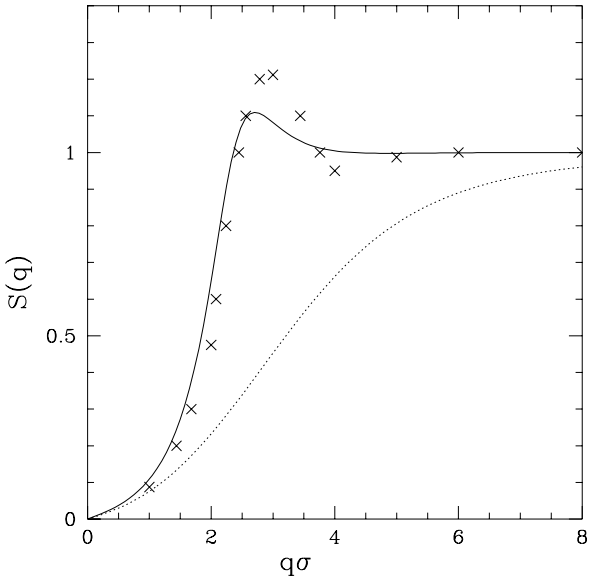

Figure 8. Structure factor $S(q)$ of the 3D-YBF at $\Lambda^* = 0.200$ and $\rho = 0.0696$: the STLS (full curve) and RPA (dotted curve) results are compared with the QMC results (crosses) of Ceperley *et al* [2].

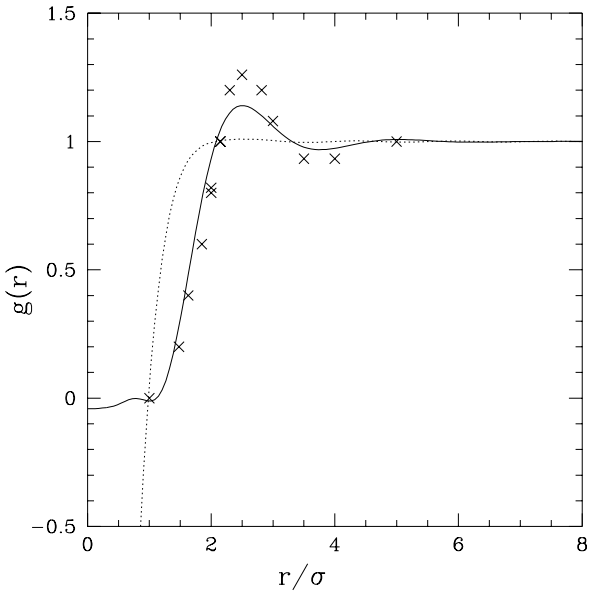

Figure 9. The same as in figure 8, for the pair distribution function $g(r)$.

4. Ground-state energy

As a first step in the evaluation of the internal energy of the 3D-YBF and 2D-YBF at $T = 0$, we calculate their potential energy u_0 (per particle and in units of the energy scale ε) from

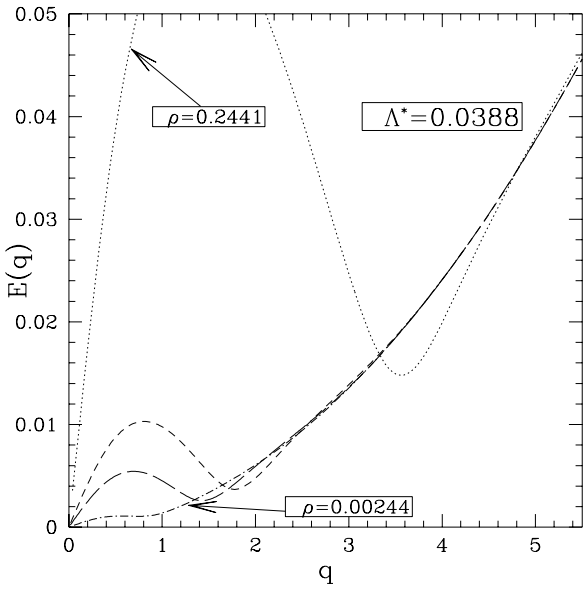

Figure 10. Dispersion curve of the collective mode in the 3D-YBF at $\Lambda^* = 0.0388$ and $\rho = 0.2441$, 0.0244, 0.0122 and 0.002 44 (from top to bottom curve).

the expression

$$u_D = 2^{D-2}\pi\rho + c_D \int_0^\infty q^{D-1}\,\mathrm{d}q\,\frac{S(q)-1}{1+q^2} \tag{23}$$

with $c_3 = 1/\pi$ and $c_2 = 1/2$. Scaled wavenumbers are used in the integral in equation (23). The first term in the right-hand side of this equation is the Hartree value of the interaction energy, given by $nV_D(q=0)/2$.

The ground-state energy E_{gs} can then be evaluated by an integration over the coupling constant λ,

$$E_{gs} = \int_0^1 \mathrm{d}\lambda\,\frac{u(\lambda)}{\lambda} \tag{24}$$

where $u(\lambda)$ refers to a modified Hamiltonian $H(\lambda) = K + \lambda P$ with K and P the kinetic and the potential energy, respectively. In our approach this implies using in equation (23) a coupling-constant-dependent structure factor $S(q;\lambda)$, which is determined self-consistently with a coupling-constant-dependent local field factor $G(q;\lambda)$ from equations (11) and (12).

Numerical convergence in the solution of the STLS self-consistency equations is not easily achieved for the values of the system parameters of present interest. In the case $D = 3$ we have obtained convergence for each of the values of (Λ^*, ρ) studied in the QMC work [2], when we used $G(q;\lambda)$ as input for the first self-consistency cycle in the evaluation of $G(q;\lambda+\Delta\lambda)$. For the 2D-YBF we could not achieve convergence at the lowest values of (Λ^*, ρ) examined by Magro and Ceperley [3], and in the case $(\Lambda^* = 0.032,\ \rho = 0.01)$ convergence required moving adiabatically with ρ and was too slow to allow a calculation of the ground-state energy.

Our results for the ground-state energy are reported in table 1 for the 3D-YBF and in table 2 for the 2D-YBF. The overall agreement with the QMC data [2, 3] is quite good, as can be seen from these tables. It is somewhat better in the case $D = 3$ and in both

dimensionalities it improves as the reduced density increases. It should also be remarked that for most pairs of system parameters shown in tables 1 and 2 the neglect of short-range correlations in the RPA leads to *negative* values of the ground-state energy. This nonsensical result reflects the large negative values of the RPA pair distribution function that we have illustrated in figure 9.

Table 1. Ground-state energy of the 3D-YBF (in units of ε) for various values of the DeBoer parameter Λ^* and of the reduced density ρ. The STLS results are compared with the variational Monte Carlo (VMC) results of Ceperley *et al* [2].

Λ^*	ρ	STLS	VMC
0.038 8261	0.002 44	0.001 27	0.001 23
0.038 8261	0.003 66	0.002 53	0.002 40
0.038 8261	0.004 88	0.004 15	0.003 99
0.038 8261	0.0122	0.0190	0.017 62
0.038 8261	0.0244	0.0553	0.0519
0.038 8261	0.2441	1.12	1.10
0.054 8068	0.006 10	0.007 06	0.006 70
0.054 8068	0.008 84	0.0127	0.0121
0.054 8068	0.012 21	0.0210	0.0199
0.054 8068	0.0298	0.0780	0.074 46
0.054 8068	0.2441	1.14	1.122
0.054 8068	1.133	6.29	6.262
0.060 6588	0.0292	0.0773	0.0749
0.060 3212	0.0696	0.248	0.240
0.060 6588	0.2441	1.145	1.142
0.060 3212	0.4883	2.52	2.495
0.070 7874	0.0293	0.0801	0.077 47
0.070 7874	0.0696	0.252	0.2460
0.070 7874	0.2441	1.15	1.142

Table 2. Ground-state energy of the 2D-YBF (in units of ε) for various values of Λ^* and ρ. The STLS results are compared with the diffusion Monte Carlo (DMC) results of Magro and Ceperley [3].

Λ^*	ρ	STLS	DMC
0.058	0.02	4.03×10^{-3}	3.085×10^{-3}
0.065	0.02	4.34×10^{-3}	3.397×10^{-3}
0.065	0.03	1.06×10^{-2}	8.293×10^{-3}
0.075	0.03	1.13×10^{-2}	9.068×10^{-3}
0.085	0.065	5.54×10^{-2}	4.69×10^{-2}
0.112	0.065	5.92×10^{-2}	5.27×10^{-2}
0.069	0.135	0.179	0.163
0.088	0.135	0.185	0.172
0.05	0.4	0.826	0.799
0.1	0.4	0.865	0.847

5. Pressure and compressibility

The pressure and the compressibility can be written in terms of the first and second derivative of E_{gs} with respect to the density ρ. As remarked in section 2, the compressibility can also

be evaluated from the speed of sound and from the static density response function (see equation (6)). Consistency between the latter value and the thermodynamic value obtained from the second density derivative of E_{gs} is known as the compressibility sum rule.

In evaluating the density dependence of E_{gs} we found it convenient to evaluate first the density dependence of the structure factor $S(q;\lambda)$ and to then use the first two density derivatives of this function in equations (23) and (24). These two quantities are obtained by solving the integral equations

$$\frac{\partial S(q,\lambda)}{\partial \rho} = -A_D(q)S^3(q,\lambda)\left[1 + \int_0^\infty \mathrm{d}k B(q,k)\frac{\partial S(k,\lambda)}{\partial \rho}\right] \tag{25}$$

and

$$\frac{\partial^2 S(q,\lambda)}{\partial \rho^2} = -A_D(q)S^3(q,\lambda)\int_0^\infty \mathrm{d}k B_D(q,k)\frac{\partial^2 S(k,\lambda)}{\partial \rho^2} + \frac{3}{S(q,\lambda)}\left[\frac{\partial S(q,\lambda)}{\partial \rho}\right]^2 \tag{26}$$

where

$$A_D(q) = \frac{2^{D-1}\pi\lambda}{\Lambda^{*2}q^2(1+q^2)} \tag{27}$$

and

$$B_D(q,k) = \frac{1+q^2}{q^2}k^{D-1}\Pi_D(q,k). \tag{28}$$

Equations (25) and (26) are Fredholm integral equations of the second kind. We found that, while a self-consistent method of solution converges, the solution of these equations by a diagonalization procedure is computationally faster.

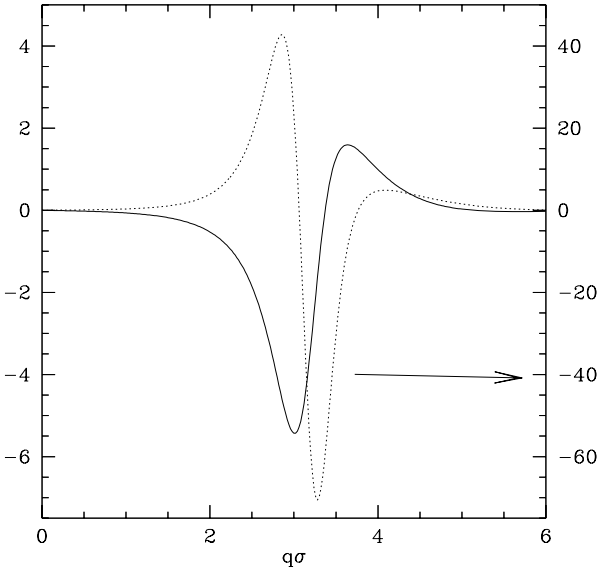

Figure 11. First and second density derivative of the structure factor $S(q)$ versus $q\sigma$ for the 2D-YBF at $\Lambda^* = 0.05$ and $\rho = 0.4$: $\partial S(q)/\partial\rho$ is given by the solid line with the scale on the left, $\partial^2 S(q)/\partial\rho^2$ by the dotted line with the scale on the right.

Figure 11 reports the values of $\partial S(q)/\partial\rho$ and $\partial^2 S(q)/\partial\rho^2$ for the 2D-YBF at ($\Lambda^* = 0.05$, $\rho = 0.4$). Of course, these functions are strongly structured in the neighbourhood of the main peak of $S(q)$.

The pressure P is evaluated from the expression

$$P = \rho^2 \int_0^1 \mathrm{d}\lambda \frac{\partial u_D(\lambda)}{\partial \rho} \tag{29}$$

where

$$\frac{\partial u_D(\lambda)}{\partial \rho} = 2^{D-2}\pi + c_D \int_0^\infty \mathrm{d}q \frac{q^{D-1}}{1+q^2} \frac{\partial S(q,\lambda)}{\partial \rho}. \tag{30}$$

Similar expressions are easily obtained for the thermodynamic compressibility.

Table 3. STLS values of the pressure (in units of ε/σ^3) and the compressibility (in units of σ^3/ε) of the 3D-YBF at $T = 0$, for various values of Λ^* and ρ.

			Compressibility	
Λ^*	ρ	Pressure	From $E_{gs}(\rho)$	From G_0
0.038 8261	0.002 44	5.2×10^{-6}	7.1×10^4	11×10^4
0.038 8261	0.003 66	1.6×10^{-5}	2.3×10^4	3.6×10^4
0.038 8261	0.004 88	3.4×10^{-5}	1.1×10^4	1.6×10^4
0.038 8261	0.0122	3.68×10^{-4}	1.08×10^3	1.46×10^3
0.038 8261	0.0244	1.98×10^{-3}	214	265
0.038 8261	0.2441	0.320	1.49	1.57
0.054 8067	0.006 10	6.8×10^{-5}	5.7×10^3	8.2×10^3
0.054 8067	0.008 84	1.7×10^{-4}	2.3×10^3	3.1×10^3
0.054 8067	0.012 21	3.9×10^{-3}	1.0×10^3	1.4×10^3
0.054 8067	0.0298	3.26×10^{-2}	132	161
0.054 8067	0.2441	0.322	1.48	1.57
0.054 8067	1.133	7.62	6.42×10^{-2}	6.58×10^{-2}
0.060 6587	0.0292	3.1×10^{-3}	1.3×10^2	1.6×10^2
0.060 3211	0.0696	2.21×10^{-2}	20.6	23.3
0.060 6587	0.2441	0.323	1.47	1.57
0.060 3211	0.4883	1.36	0.355	0.370
0.070 7873	0.0293	3.2×10^{-3}	135	164
0.070 7873	0.0696	2.23×10^{-2}	20.4	23.2
0.070 7873	0.2441	0.324	1.47	1.56

Our results for the pressure and the compressibility are shown in table 3 for the 3D-YBF and in table 4 for the 2D-YBF. A test against QMC data can be given only for the pressure in the 2D-YBF and the degree of agreement with the results of Magro and Ceperley [3] in table 4 appears to be quite reasonable. In both tables the violation of the compressibility sum rule is tested by reporting the values of the compressibility obtained from the density dependence of the ground-state energy and from the speed of sound. The differences between these two sets of values are quite small at high density, but progressively increase with decreasing density.

6. Summary and conclusions

We have examined in this work the usefulness of the STLS approach in describing the consequences of short-range correlations in the ground-state properties of the two-dimensional and three-dimensional Yukawa Bose fluids. Our attention has been mainly focused on the calculation of the thermodynamic properties of these fluids at zero temperature, for which we have reported extensive sets of numerical values and tested them against Monte Carlo data wherever possible.

Table 4. Pressure (in units of ε/σ^2) and compressibility (in units of σ^2/ε) of the 2D-YBF at $T = 0$. The STLS values of the pressure are compared with the DMC results of Magro and Ceperley [3].

		Pressure		STLS compressibility	
Λ^*	ρ	STLS	DMC	From $E_{gs}(\rho)$	From G_0
0.058	0.02	1.82×10^{-4}	1.32×10^{-4}	1.68×10^{3}	3.43×10^{3}
0.065	0.02	1.92×10^{-4}	1.43×10^{-4}	1.62×10^{3}	3.27×10^{3}
0.065	0.03	6.82×10^{-4}	5.27×10^{-4}	4.83×10^{2}	8.76×10^{2}
0.075	0.03	7.11×10^{-4}	5.58×10^{-4}	4.67×10^{2}	8.39×10^{2}
0.085	0.065	6.36×10^{-3}	5.65×10^{-3}	60.1	88.2
0.112	0.065	6.69×10^{-3}	6.07×10^{-3}	58.3	85.1
0.069	0.135	0.0382	0.0359	11.1	14.0
0.088	0.135	0.0389	0.0372	10.9	13.8
0.05	0.4	0.431	0.426	1.08	1.19
0.1	0.4	0.441	0.439	1.06	1.18

From these comparisons it appears that the STLS results have almost fully quantitative value for the thermodynamic properties of the fluid phase on the high-density side of the solid phase and provide a useful starting point for more quantitative studies of the low-density fluid. It may also be noticed that the dielectric approach as developed in this work can easily be extended to deal with equilibrium states at finite temperature.

Improvements in the present approach can be sought in two main directions. Firstly, a fully quantitative account of the thermodynamic compressibility sum rule can be imposed through a further self-consistency requirement and may be relevant for an evaluation of the crystal-to-superfluid phase boundary. Secondly, the inclusion of higher dynamic correlations via a frequency-dependent local field factor will be crucial for a correct description of excitation spectra.

References

[1] Ceperley D M, Chester G V and Kalos M H 1976 *Phys. Rev.* D **13** 3208
[2] Ceperley D M, Chester G V and Kalos M H 1978 *Phys. Rev.* D **17** 1070
[3] Magro W R and Ceperley D M 1993 *Phys. Rev.* B **48** 411
[4] Baym G and Pethick C J 1975 *Ann. Rev. Nucl. Sci.* **25** 27
[5] Nelson D R and Seung H S 1989 *Phys. Rev.* B **39** 9153
[6] Minnhagen P 1998 *Models and Phenomenology for Conventional and High-Temperature Superconductors, Proc. 136th Course E Fermi School* ed G Iadonisi, J R Schrieffer and M L Chiofalo (Bologna: Societá Italiana di Fisica)
[7] Xing L and Tesanovic Z 1990 *Phys. Rev. Lett.* **65** 794
[8] Ma H-R and Chui S T 1991 *Phys. Rev. Lett.* **67** 505
[9] Sengupta S, Dasgupta C, Krishnamurthy H R, Menon G I and Ramakrishnan T V 1991 *Phys. Rev. Lett.* **67** 3444
[10] Menon G I, Dasgupta C, Krishnamurthy H R, Ramakrishnan T V and Sengupta S 1996 *Phys. Rev.* B **54** 16 192
[11] Nordborg H and Blatter G 1997 *Phys. Rev. Lett.* **79** 1925
[12] Singwi K S, Tosi M P, Land R H and Sjölander A 1968 *Phys. Rev.* **176** 589
[13] Gold A 1992 *Z. Phys.* B **89** 1
[14] Conti S, Chiofalo M L and Tosi M P 1994 *J. Phys.: Condens. Matter* **6** 8795
[15] Moudgil R K, Ahluwalia P K, Tankeshwar K and Pathak K N 1997 *Phys. Rev.* B **55** 544
[16] Strepparola E and Tosi M P 1998 *Mod. Phys. Lett.* B **12** 459
[17] Bulutay C, Tanatar B and Tomak M 1998 *Phys. Rev.* B **57** 15 197
[18] Chiofalo M L, Conti S and Tosi M P 1994 *Mod. Phys. Lett.* B **8** 1207